Journal of Hazardous Materials 188 (2011) 58–66

Contents lists available at ScienceDirect

Journal of Hazardous Materials

journal homepage: www.elsevier.com/locate/jhazmat

Physicochemical properties of metal-doped activated carbons and relationship with their performance in the removal of SO_2 and NO

Xiang Gao*, Shaojun Liu, Yang Zhang, Zhongyang Luo, Kefa Cen

State Key Laboratory of Clean Energy Utilization, Zhejiang University, 38 Zheda Road, Hangzhou 310027, PR China

ARTICLE INFO

Article history:
Received 22 July 2010
Received in revised form 13 January 2011
Accepted 14 January 2011
Available online 22 January 2011

Keywords:
Activated carbon
Metal oxide
Physicochemical
Removal

ABSTRACT

Several metal-doped activated carbons (Fe, Co, Ni, V, Mn, Cu and Ce) were prepared and characterized. The results of N_2 adsorption–desorption, X-ray diffraction, and X-ray photoelectron spectroscopy indicated that some metals (Cu and Fe) were partly reduced by carbon during preparation. Activity tests for the removal of SO_2 and the selective catalytic reduction of NO with ammonia were carried out. Due to different physicochemical properties, different pathways for the SO_2 removal had been put out, i.e., catalytic oxidation, direct reaction and adsorption. This classification depended on the standard reduction potentials of metal redox pairs. Samples impregnated with V, Ce and Cu showed good activity for NO reduction by NH_3, which was also ascribed to the reduction potential values of metal redox pairs. Ce seemed to be a promising alternative to V due to the higher activity in NO reduction and the nontoxic property. A metal cation which could easily convert between the two valences seemed to be crucial to the good performance of both SO_2 and NO removal, just like V and Cu.

1. Introduction

Activated carbons are industrially applied in many processes either as catalyst or as adsorbent. Among these processes, carbon-based flue gas cleaning attracts worldwide interest. The first technique for dry NO and SO_2 removal using activated carbons was developed in the 1960s by Bergbau and commercialized by Mitsui-Bergbau Forschung [1]. However, in this process carbons should be applied at low space velocity because of their low activities for NO and SO_2 removal. An enhancement of this activity is required through a proper modification of the carbon characteristics and use of additives [2]. The SO_2 removal activity enhancement for various carbons by incorporated oxides of V [3–5], Fe [4,6,7], Co [4,5], Ni [4,5], Mn [4,5] and Cu [8] has been reported. Meanwhile, NO reduction over carbon-based catalysts doped with oxides of V [9–11], Mn [11–13], Fe [11,14,15], Cu [14,16] and Ni [11] has been studied and promising results have been obtained.

Also, there have been attempts to relate the removal performance to physicochemical characteristics of the metal-doped carbons. As for SO_2 removal, Lopez proposed that copper oxides had a catalytic effect toward the transformation of SO_2 into other species [17]. Liu revealed that Fe_2O_3 reacted with SO_2 resulting in the formation of H_2SO_4 and $Fe_2(SO_4)_3$ [7]. Liu also suggested that V_2O_5 chemically absorbed SO_2 to form a $VOSO_4$-like intermediate [3]. Li and Henrich gave the evidence of associative SO_2 adsorption on NiO by XPS [18]. When studying the connection between metal oxides and NOx removal, there were similar opinions that metal oxides drastically enhanced activities. As suggested by Bandosz, cerium (III) can get oxidized by NO_2, bind nitrogen as $Ce(NO_3)_4$ and then further oxidize the carbon surface [19].

However, it is difficult to compare results from different studies, due to varying preparation procedures and testing conditions. So it is necessary that all the carbons are doped with equivalent amount of oxides by the same method and exposed to the reaction gas for equal time as well as at the same temperature. It is thus possible to compare the effect of metal oxides on the NO and SO_2 removal activities over carbons.

The main objective of this work is to try to advance in the understanding of physicochemical properties of the metal-doped activated carbons and clarify the effect of different metal oxides on the SO_2 and NO removal under the same conditions. Based on these results, the promising metal will be selected for the removal of SO_2 and NO.

2. Experiment

2.1. Carbon sample preparation

An activated carbon (AC) was obtained from Tangshan Huaneng Technology Carbon Company, which was derived from the mixture of coal and coconut shell. The active metals in this study were Fe, Co, Ni, V, Mn, Cu and Ce. The deposition of the metal oxides

* Corresponding author. Tel.: +86 571 87951335; fax: +86 571 87951616.
E-mail address: xgao1@zju.edu.cn (X. Gao).

0304-3894/$ – see front matter © 2011 Elsevier B.V. All rights reserved.
doi:10.1016/j.jhazmat.2011.01.065

Table 1
Elemental and proximate analyses of AC.

Material	Elemental analysis [wt.%]					Proximate analysis [wt.%]			
	C	H	O[a]	N	S	Moisture	Ash	Volatile	Fixed carbon
AC	73.44	0.76	5.06	0.62	0.37	10.51	9.24	5.12	75.13

[a] By difference.

was achieved by impregnating the carbon with an aqueous metal oxide precursor solution, denoted as incipient wetness impregnation. Metal nitrate salts were preferably used as precursors to make the different samples as equivalent as possible. However, in the case of vanadium, ammonium metavanadate was dissolved in oxalic acid. The concentrations of the precursor solutions were chosen so that the impregnation could be preformed by adding equal volume of solutions to 5 g AC. At last, 1.11 mmol/g AC of metals, corresponding to 3 wt.% Ce, were added to the carbon. Subsequently, the water evaporated by heating the samples to about 50 °C in a vacuum drying oven for 24 h. The samples were then calcined at 800 °C for 15 min in inert atmosphere, as suggested by Davini [4]. Finally, the samples were denoted as X-AC, where X indicated the metal used and AC was the activated carbon (Table 1).

2.2. Activity tests of samples

SO_2 and NO removal tests were performed in an experimental installation built for this purpose. Two different feed gas compositions were used, i.e., $feed_{SO_2}$ ($SO_2 + O_2 + H_2O + N_2$) and $feed_{NO}$ ($NO + NH_3 + O_2 + Ar$), as presented in Table 2. In all runs, the flow rate was maintained at 0.4 L/min, and 1 g sample (particle size, 30–60 mesh) was placed above a quartz wool layer in the middle of the reactor. In the SO_2 removal tests, $feed_{SO_2}$ gas mixtures were passed for 2 h through the reactor, which held the temperature constant at 150 °C. The amount of SO_2 retained by the carbons was determined by the integration of the breakthrough SO_2 curve [20]. After the adsorption step, the desorption step was carried out. This involved inserting the reactor into an oven already heated at 360 °C and flowing nitrogen (50 ml/min for 1 h). The desorbed gas flowed through the scrubbing bottle, which contained 250 ml hydrogen peroxide (5 vol.%), after a procedure reported in literature [6]. The sulfuric acid, obtained by the oxidation of the desorbed SO_2, was then detected by an ion chromatography (after diluted).

In the NO removal tests, the samples were first exposed to $feed_{NO}$ gas mixtures at 100 °C until a stable concentration level of the outlet gas was achieved. And then, the temperature was raised by 20 °C to the next temperature level until 200 °C.

2.3. Characterization of samples

Nitrogen adsorption–desorption isotherms were measured on a Quantachrome Autosorb-1-C at 77 K. Total surface area was determined using the Brunauer–Emmett–Teller (BET) equation. The micropore width and micropore volume were calculated by applying the Dubinin–Radushkevich (DR) equation.

Proximate analysis of the as-received activated carbon was performed according to GB/T 212-2001 standard for coal and ultimate analysis was carried out in a LECO CHNS 932. Pertinent results are shown in Table 1. In order to identify the mineral components in the sample, the ash was analyzed by X-ray fluorescence (XRF) in a Rigaku-ZSX100e.

Powder X-ray diffraction (XRD) patterns were collected with X′Pert PRO diffractometer using Cu Kα radiation source. A continuous mode was used to collect data from 10° to 90° of 2θ at a scanning speed of 10°/min.

X-ray photoelectron spectroscopy (XPS) was used to study the chemical composition of the carbon surface. Photoelectron spectra were recorded with a VG ESCALAB MARK II electron spectrometer equipped with an MgKα X-ray source ($h\nu$ = 1253.6 eV) and a hemispherical electron analyzer operating at a constant pass energy (50 eV). Accurate (±0.1 eV) binding energies were determined with respect to the position of the C1s peak at 284.5 eV. According to the literature [21], the peaks were deconvoluted after subtraction of the Shirley background by using a sum of Lorentzian/Gaussian functions, fixing the width at half height equal to 2 eV.

Table 3
Textural characterization of the samples.

Sample	BET surface area (m^2/g)	DR micropore volume (ml/g)	DR micropore width (nm)
AC	702	0.36	1.0
Fe-AC	621	0.32	1.1
Co-AC	824	0.42	1.2
Ni-AC	802	0.41	1.1
V-AC	789	0.40	1.1
Mn-AC	708	0.36	1.1
Cu-AC	730	0.37	1.2
Ce-AC	607	0.31	1.1

3. Results and discussion

3.1. Textural characterization

The textural characterization of the samples is presented in Table 3. It can be seen that both the BET surface area and micropore volume increased after the deposition of the metal oxides except the samples Fe-AC and Ce-AC. The increase in porosity could be attributed to the decomposition of the oxygen functional groups during the calcinations under 800 °C, such as carboxylic acids (which decomposed at 140 °C), lactones (decomposing between 200 and 600 °C), carboxylic anhydrides (decomposing at 675 and 740 °C), and carbonyls, ether and quinines (decomposing at 750 °C) [19]. Moreover, the reduction of metal species (see below) can also produce an increase in porosity due to carbon gasification. However, the adsorption of metals on the external surface and the aggregation of particles to form large crystals on heat treatment may result in the significant decrease of micropores, especially in the case of Fe-AC and Ce-AC [22,23]. The increase of micropore width for all metal doped samples verified this deduction.

Table 2
Compositions of the feed gas.

Feed gas abbreviation	[NO] (ppm)	[SO_2] (ppm)	[NH_3] (ppm)	[O_2] (%)	[H_2O] (%)
$feed_{SO_2}$	450	1000	500	5	8
$feed_{NO}$				65	

Table 4
Ash composition analysis of AC by XRF[a].

Compound	%
Na_2O	3.61
MgO	7.86
Al_2O_3	21.6
SiO_2	33.9
Fe_2O_3	10.8
SO_3	6.36
CaO	12.3
K_2O	1.07
Others	2.5

[a] Others: BaO, P_2O_5, TiO_2, SrO, MnO.

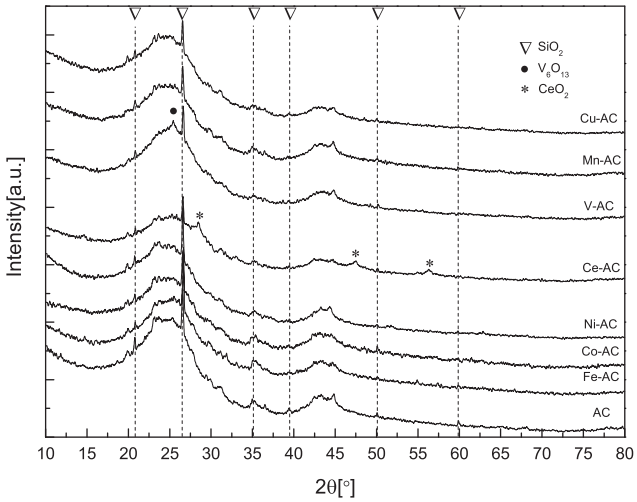

Fig. 1. X-ray diffraction patterns of different samples.

3.2. Bulk chemistry characterization by XRF and XRD

The ash composition of the as-received activated carbon obtained by XRF is shown in Table 4. The main oxides present in the ash were silica, alumina, iron oxides and calcium oxides, which corresponded to their main mineral phases (quartz, clays, pyrite and gypsum) [24]. The ash also contained small percentages of alkali and alkali-earth metal oxides, as well as titanium oxides.

Fig. 1 shows the XRD patterns of different samples. All of the samples, with or without metal oxides in the matrix, exhibited two broad bands around $2\theta = 24^\circ$ and 43°, corresponding to amorphous carbon structure [25,26]. Together with these bands, the XRD diffraction peaks corresponding to SiO_2 (at $2\theta = 20.8^\circ$, 26.6°, 36.5°, 39.4°, 50.0° and 59.9°) also appeared. The above results are in agreement with the XRF findings, which indicate that the SiO_2 is the major mineral components in the samples, derived from the as-received AC, as shown in Table 4. The mean particle size of SiO_2 was about 57 nm. This particle size was calculated from Scherer's equation applied to the half-height of the maximum intensity diffraction peak [26]. For sample V-AC, a strong diffraction peak at $2\theta = 25.3^\circ$ was observed. Due to its high intensity and the narrow band width, phase identified was V_6O_{13}, suggesting a poor dispersion of metal oxide particles on the V-AC sample. The similar phenomenon was also observed on the sample Ce-AC (peaks corresponding to CeO_2 at $2\theta = 28.5^\circ$, 47.4° and 56.2°). However, the other samples impregnated with different metals did not show any diffraction peak corresponding to the metal oxide phase, implying that these phases are well dispersed on the carbon matrix.

Table 5
Monolayer dispersion capacity based on the model of close monolayer dispersion (mmol/702.2 m^2 (surface area of 1 g AC support)).

Fe_2O_3	11.44
CoO	17.17
NiO	17.17
CeO_2	8.59
V_2O_5	6.87
MnO	17.17
CuO	17.17

The possible reasons for the poor dispersion of V and Ce on the activated carbon were as follows: First, for an oxide dispersed on a support, there is a monolayer dispersion capacity. When its loading is lower than the capacity, the oxide will be in a monolayer state. While its loading exceeds the capacity, the surplus oxide will remain as crystalline phase in the system together with its monolayer phase and may be detected by XRD. According to the literature [27], the monolayer capacities were calculated for all metals used, as shown in Table 5. 1.11 mmol/g AC of metal was added to the carbon, below the values calculated. However, this method is an approximate theory calculation, that is to say, the crystal may still form even the actual loading is below the calculated monolayer dispersion capacity. For the metals investigated, Ce and V had the lower monolayer dispersion capacities. It may be the reason for the poor dispersion of V and Ce on the activated carbon.

Moreover, as suggested by Baxter, vanadia species may have significant mobility on TiO_2 or other oxide surfaces [28]. At relatively high vanadia concentrations, it may become easier for the vanadia species to agglomerate. It indicates that the same phenomenon may also occur on carbon surface.

Table 6
Deconvolution of metal 2p core-level spectra before and after SO_2 removal.

Sample	$2p_{3/2}$ binding energy (eV)		Interpretation			
	Before reaction	After SO_2 removal	Before reaction	Reference	After SO_2 removal	Reference
Fe-AC	708.4	710.6	FeO	[29]	Fe_2O_3	[29]
	709.6	712.4	FeO	[29]	$FeSO_4/Fe_2(SO_4)_3$	[33]
	711.2	714.1	Fe_2O_3	[29]	$FeSO_4/Fe_2(SO_4)_3$	[33]
Co-AC	779.6	781.4	CoO	[32]	$CoO/Co(OH)_2$	[31]
	781.9	784.1	$CoO/Co(OH)_2$	[31]	$CoSO_4$	[5]
	787	787.4	$CoO/Co(OH)_2$	[31]	$CoO/Co(OH)_2$	[31]
Ni-AC	855.3	856.7	$Ni(OH)_2/NiO$	[33]	NiO	[33]
	860.6	861.4	NiO	[30]	NiO	[30]
V-AC	517.3	517.1	V_2O_5	[32,34]	V_2O_5	[32,34]
Mn-AC	641.5	642.7	MnO	[33]	$MnSO_4$	[33]
Cu-AC	931.8	934.6	Cu_2O	[33]	CuO	[33]
	933.4	936.9	CuO	[32]	$CuSO_4$	[33]

Table 7
Binding energy values (eV) of Ce 3d components, full-width at half maximum (FWHM) values, and Ce^{3+}/Ce_{tot} atomic ratio before and after SO_2 removal.

Peak	Position (eV)	FWHM (eV)	Ce^{3+}/Ce_{tot} [a] (at.%)	
			Before reaction	After SO_2 removal
V	882.2	2.8	0.08	0.30
U	900.7	2.6		
V″	888.6	6.4		
U″	907.2	6.8		
V‴	898.0	2.9		
U‴	916.15	2.9		
V′	884.4	2.1		
U′	903.9	1.8		

[a] $Ce^{3+}/Ce_{tot} = Ce^{3+}/(Ce^{4+} + Ce^{3+})$.

3.3. Surface chemistry characterization by XPS

XPS tests for the different carbons were carried out, recording the N1s, C1s, metal 2p or 3d (Ce) core-level spectra. No significant peak was found for the N1s spectra, indicated that all the nitrates were totally decomposed during the preparation.

Results of the XPS studies of the metal core-level spectra are shown in Fig. 2. The deconvolutions of metal core-level spectra are compiled in Tables 6 and 7.

Fe $2p_{3/2}$ spectrum comprised the peaks at 711.2 eV (49%), 709.6 eV (30%) and 708.4 eV (21%). The binding energy (BE) value of the first peak (711.2 eV) was in the range of literature data for Fe^{3+} (710.8–711.8 eV); the last two (709.6 and 708.4 eV) might be ascribed to a reduced chemical form of iron like Fe^{2+} (708.7–707.1 eV) [29]. Thus, iron ions in the sample could be reduced by carbon during the calcinations at 800 °C.

The XPS pattern of the Co $2p_{3/2}$ region was qualitatively very similar to that reported elsewhere [30]. The first component of the Co $2p_{3/2}$ region at 781.9 eV and a typical satellite feature detected at around 787 eV (785.2 eV) suggested a Co(II) oxide/hydroxide composition [31]. The second component at 779.6 eV could be due to CoO, reported to have BE values between 779.5 and 780 eV [32].

The Ni $2p_{3/2}$ region had two components at 855.3 and 860.6 eV. The first component at 855.3 eV could be due to either $Ni(OH)_2$, which had a BE between 855.3 and 856.6 eV, or NiO, with a BE in the range of 853.5–857.2 eV [33]. The other component at higher BE corresponded to a satellite of the main peak characteristic of a Ni(II)–O bond [30].

The Cu $2p_{3/2}$ region was composed of two components at 933.4 eV (30%) and 931.8 eV (70%). The BE of Cu $2p_{3/2}$ in copper(II) oxide was 933.6 eV [32]. Therefore, in our case the component peak at 933.4 eV was more likely due to copper oxide. The second component at 931.8 eV could correspond to the Cu_2O, BE value of 932 eV [33], due to the reduction of copper(II) precursor by carbon, as in the case of the Fe^{3+} ions. The same phenomenon was also observed by Pasel et al. [14].

The Mn $2p_{3/2}$ region consisted of one peak at 641.5 eV, which compared to 640.4–642.5 eV for MnO [33], verified $Mn(NO_3)_2$ was totally decomposed.

The binding energy of V $2p_{3/2}$ was 517.3 eV, indicating that vanadium is in oxidation state +5 in the sample [32,34]. The oxidation of precursor could be considered to be caused by the addition of oxalic acid, which served as oxidant during the sample preparation. However, due to the absence of the oxidant, other metals kept the initial state or even were reduced by carbon, like Fe and Cu.

The oxidation states of surface cerium species on sample Ce-AC was characterized by XPS analysis. The Ce 3d XPS spectra of Ce (IV) could be resolved into six features. If some Ce (III) species were present, then two more peaks and the corresponding satellites were added [35]. The curve was fitted with eight peaks, corresponding to four pairs of spin–orbit doublets, following the procedure developed by Larachi et al. [36]. The relative percentage of the two cerium species was obtained by the intensity of the Ce $3d_{5/2}$ components relative to Ce^{4+} (V, V″, V‴) and to Ce^{3+} (V′) [37]. The experimental and fitted Ce 3d spectra of sample Ce-AC are shown in Table 7 and Fig. 2. The major amounts of Ce(IV) suggested that the $Ce(NO_3)_3$ precursor decomposed into CeO_2 in inert atmosphere. However, the minor amounts of Ce(III) might be due to the transfer of electrons from the activated carbon basal planes to the metal oxide, according to the literature [38].

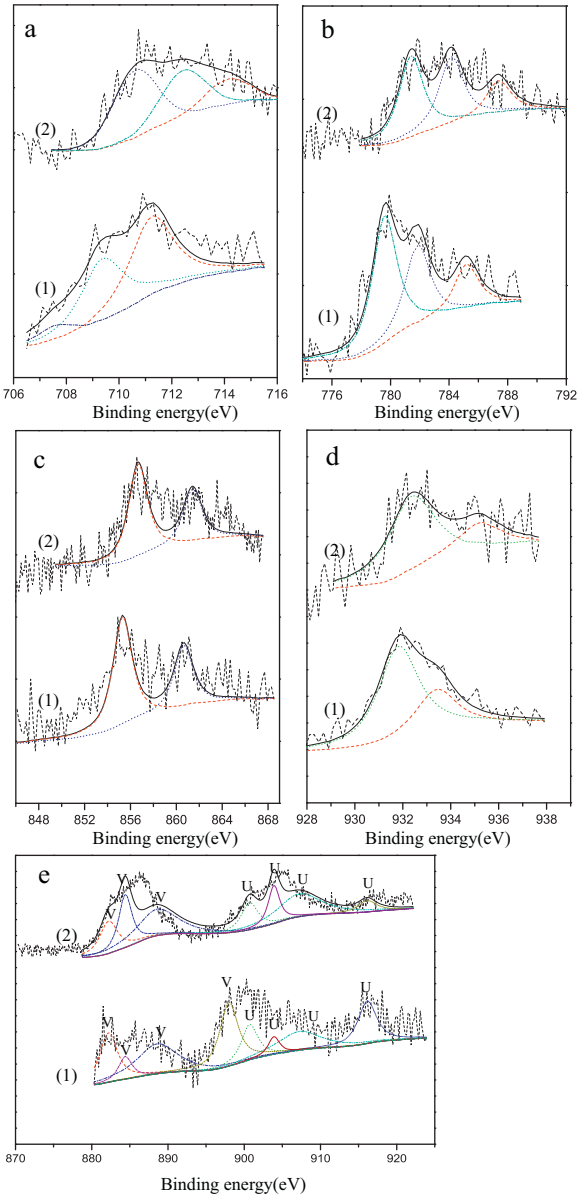

Fig. 2. Curve-fitted metal $2p_{3/2}$ or 3d (Ce) core-level spectra for the different metal-doped activated carbons. Fe-AC (a), Co-AC (b), Ni-AC (c), Cu-AC (d), and Ce-AC (e) (1. before reaction; 2. after SO_2 removal tests).

3.4. SO_2 removal tests

The SO_2 removal characteristics of the samples were tested using feed gas mixture $feed_{SO_2}$ (containing SO_2, O_2 and H_2O) in the fixed bed reactor. The results are summarized in Fig. 3. Of the metals studied, vanadium seemed to be the one which most favors SO_2 sorption onto the carbon matrix, up to 65 mg/g, while less marked

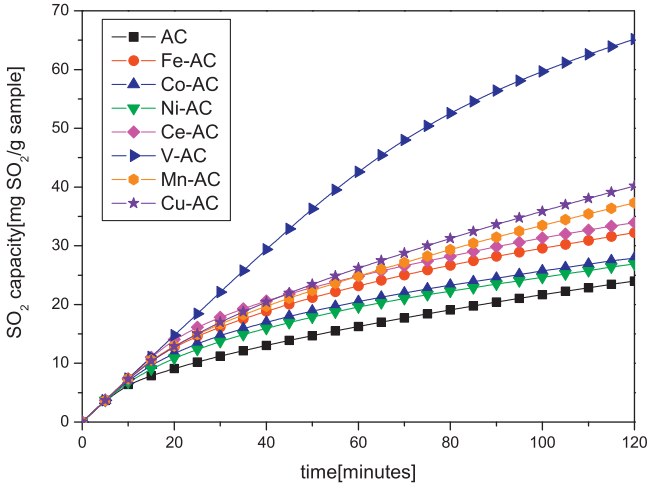

Fig. 3. SO_2 adsorption on metal-doped activated carbons from $feed_{SO_2}$ gas mixtures versus the adsorption time.

SO_2 sorption were detectable on carbons doped with other metals. Meanwhile, samples Fe-AC, Co-AC and Ni-AC exactly showed the similar adsorption characteristics due to their similar chemistry performance. The SO_2 capacity results showed an increase according to the sequence Ni-AC < Co-AC < Fe-AC. Raymundo-Piñero et al. suggested that micropores not only act as adsorption sites and contain the active sites for SO_2 oxidation, but also the adsorption potential in micropores may favour the oxidation reaction [39]. However, the surface area and micropore volume had an order of Fe-AC < Ni-AC < Co-AC. This indicates that the textural property has insignificant effect on the adsorption capacity of adsorbent. This point was confirmed by the investigation results of Davini [40], Carrascomarin et al. [41], Lizzio et al. [42], and Lee et al. [23].

Fig. 4 presents S 2p spectra taken from samples after its interaction with sulfur dioxide. To analyze these spectra in more detail and to apply literature data for comparison, we deconvoluted the S 2p lines into two components. Each S 2p peak consists of a doublet (denoted 3/2 and 1/2 for electron spin) in a ratio of 2:1 with a separation of 1.2 eV. The most intense S $2p_{3/2}$ signals appeared in a range of 168.5–169 eV for all samples, which were characteristics of sulfate types (+6) [33]. Moreover, the general trend of increasing binding energy was observed after the metal impregnation, indicating an increase in the oxidation state of sulfur according to Urban et al. [43]. This phenomenon suggests the enhancement of SO_2 removal by metal is due to the oxidation of SO_2.

The chemical state of metal was also investigated after the SO_2 removal, as shown in Fig. 2, Tables 6 and 7. The Fe $2p_{3/2}$ line was also divided into three peaks. The first peak, characteristic of the Fe(III) oxidation state, was located at 710.6 eV (48%). The other two peaks, characteristics of ferric sulfate or ferrous sulfate, were located at 712.4 eV (34%) and 714.1 eV (18%) [33].

The two components of Co $2p_{3/2}$ region (781.4 and 787.4 eV) were similar with the unreacted counterparts, while a peak at 784.1 eV was higher than the counterpart at 779.6 eV. This may lead to a conclusion that active material is present as $CoSO_4$, as suggested by Klinik and Grzybek [5].

A small change was registered for Ni $2p_{3/2}$ spectrum. Two peaks, located at 856.7 and 861.4 eV, were due to NiO and a satellite of the main peak, respectively, indicating no or only negligible reaction takes place over metal surface.

The binding energy of V $2p_{3/2}$ peak was 517.1 eV. A lower binding energy indicates an increase reduction state of V. The

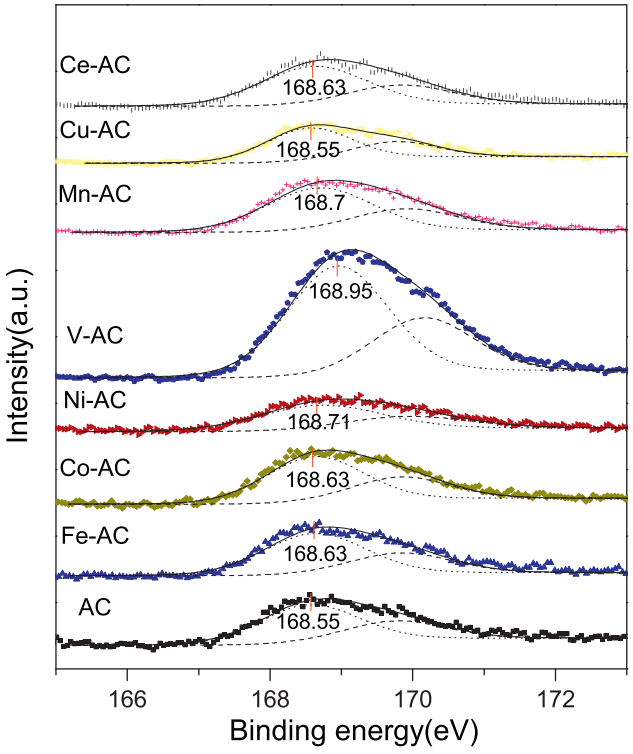

Fig. 4. The S 2p photoemission spectra recorded after the SO_2 removal tests.

change state of transition metal could play an important role in SO_2 removal.

For the reacted sample Mn-AC, a peak at 642.7 eV for the Mn $2p_{3/2}$ region was observed, which was the characteristic of $MnSO_4$ [33].

The Cu $2p_{3/2}$ line of reacted sample was also divided into two peaks. The binding energy value of the first peak (934.6 eV) was close to the literature data for CuO (932.7–934.2 eV), and the other (936.9 eV) might be ascribed to $CuSO_4$ (934.9–936 eV) [33]. The oxidation of metal was due to the SO_2 removal. As suggested by Bandosz, copper has the high propensity to form sulfates in the presence of oxygen [22].

For reacted Ce-AC, a significant increase of Ce^{3+}/Ce_{tot} was observed, indicating that part of Ce was reduced during the reaction. The electrons may come from the oxidized activated carbon.

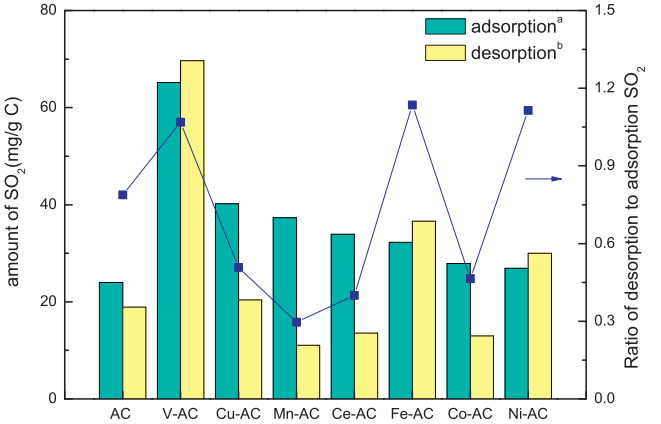

Fig. 5. Comparison between the recovered SO_2 and retained SO_2 after regeneration by thermal treatment under inert atmosphere. The higher amount of recovered SO_2 compared to retained SO_2 is due to the difference of detection methods. (a) Detected by a gas analyser and (b) detected by an ion chromatography.

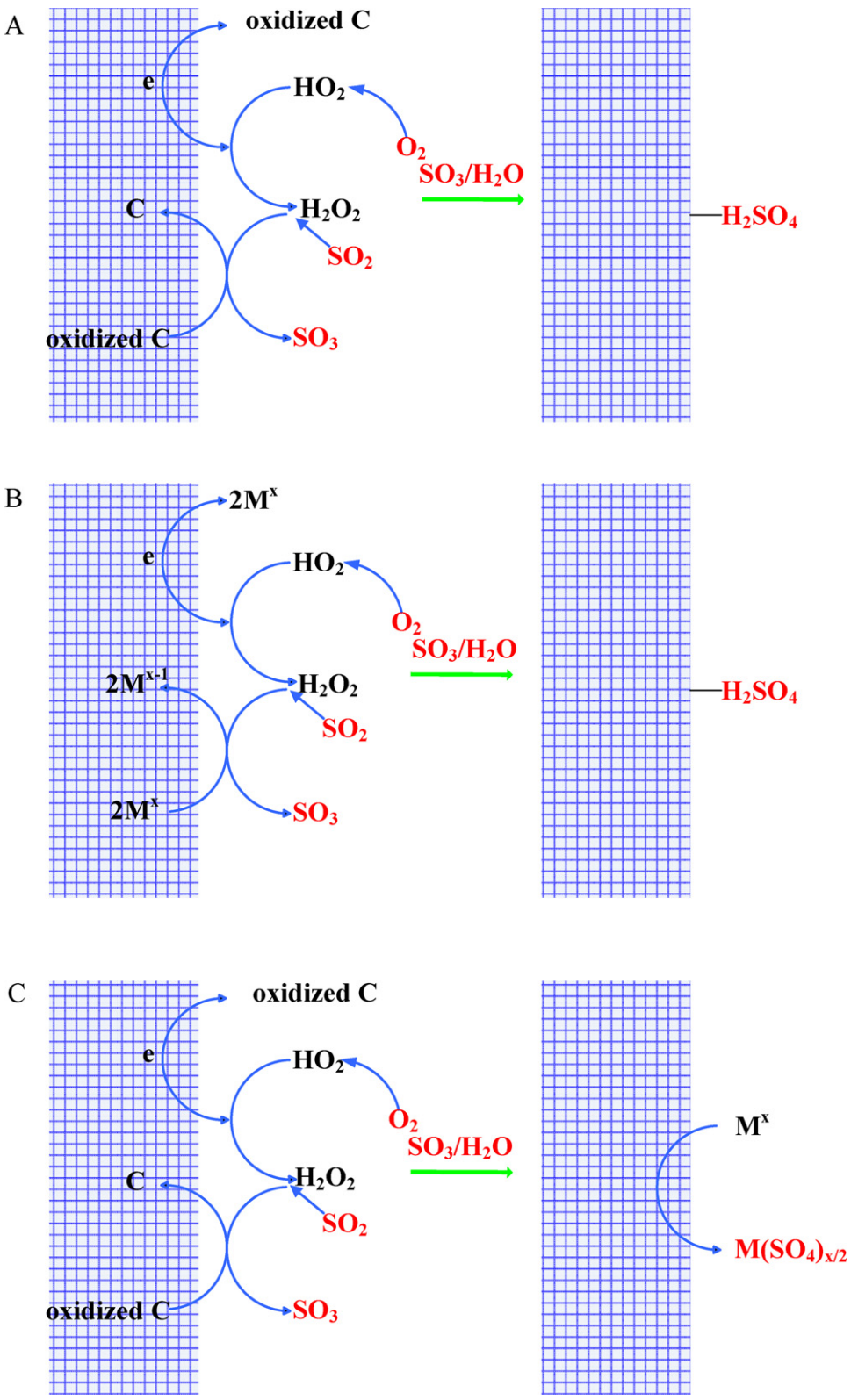

Fig. 6. Scheme showing proposed pathways for the oxidation of SO_2 onto metal-doped carbon in the presence of oxygen and water vapor: (A) catalyzed oxidation by carbon matrix; (B) catalyzed oxidation by metal oxide; (C) direct reaction with H_2O and SO_3.

In order to check the SO_2 recovery from the saturated samples, a comparison between the amount of the retained SO_2 and those recovered during regeneration of different samples is given in Fig. 5. It can be observed that the retained SO_2 was completely recovered for the samples Fe-AC, Ni-AC and V-AC. About 80% SO_2 was recovered from the saturated AC during regeneration at 360 °C. In contrast, samples Co-AC, Ce-AC, Mn-AC and Cu-AC had lower ratio of recovered SO_2 to retained SO_2, which were below 50%. These facts indicate that due to the different chemical properties of metal oxides, the retained SO_2 converts into a variety of sulfur-containing

Table 8
Standard reduction potentials [46].

Redox couple	Half-reaction	E (V)
O_2/O_2^-	$HO_2 + H^+ + e \leftrightarrow H_2O_2$	1.495
SO_4^{2-}/SO_2	$SO_4^{2-} + 4H + 2e \leftrightarrow H_2SO_3 + H_2O$	0.172
NO/N_2	$2NO + 4H^+ 4e \leftrightarrow N_2\ 2H_2O$	1.678
N_2/NH_3	$N_2 + 6H^+ 6e \leftrightarrow 2NH_3$	0.057
Fe^{3+}/Fe^{2+}	$Fe^{3+} + e \leftrightarrow Fe^{2+}$	0.777
Co^{2+}/Co	$Co^{2+} + 2e \leftrightarrow Co$	−0.28
Ni^{2+}/Ni	$Ni^{2+} + 2e \leftrightarrow Ni$	−0.257
Ce^{4+}/Ce^{3+}	$Ce^{4+} + e \leftrightarrow Ce^{3+}$	1.61
V^{5+}/V^{4+}	$V_2O_5 + 6H^+ + 2e \leftrightarrow 2VO^{2+} + 3H_2O$	0.958
Mn^{2+}/Mn	$Mn^{2+} + 2e \leftrightarrow Mn$	−1.185
Cu^{2+}/Cu	$Cu^{2+} + 2e \leftrightarrow Cu$	0.3419

complexes, a part of which are hardly recovered in the form of SO_2 at 360 °C in an inert atmosphere.

Zawadzki [44] pointed out that the superoxide ions played an important role in the catalytic oxidation of aqueous sulfur dioxide solution by O_2. Based on his theory, possible pathways for the oxidation of SO_2 onto metal-doped carbons in the presence of oxygen and water vapor had been put out, as shown in Fig. 6.

The occurrence of the pathway (B) depended on the potential differences between the metal redox couple and O_2/O_2^- couple as well as SO_4^{2-}/SO_2. According to the results of XPS, the metal redox couples were identified and their reduction potentials are listed in Table 8. For sample V-AC, since Liu [3] suggested that V_2O_5 chemically absorbed SO_2 to form a $VOSO_4$-like intermediate, the redox pair (V^{5+}/V^{4+}) was thought to be present in the reaction. For sample Cu-AC, although the presence of Cu_2O was confirmed by XPS results, Cu_2O was easily oxidized to CuO in the presence of O_2 or NO [45]. The redox pair (Cu^{2+}/Cu) was identified.

Based on Table 8, the different pathways of metal-doped carbons were clarified. The reduction potential of O_2 to O_2^- is 1.495 V, indicating that the reduction of O_2 is a feasible reaction over all the metals except Ce. However, the oxidation of SO_2 takes places only over the V, Fe, Cu and Ce, since the potential of SO_4^{2-} to SO_2 is 0.172 V. As a result, for sample V-AC, Fe-AC and Cu-AC, the pathway (B) seemed to be prevalent. For other samples except Ni-AC, the enhancement of SO_2 removal property might be due to the pathway (C). However, a part of copper oxides was involved in the pathway (C), resulting in a low ratio of recovered SO_2 to retained SO_2, as shown in Fig. 5. It was interesting to find that the retained SO_2 was completely recovered for Ni-AC, although Ni might not be involved in the catalytic oxidation of SO_2. Li and Henrich gave the evidence of the adsorption of SO_2 on NiO by XPS, and the species was presumably associative SO_2 [18]. This gave a reasonable interpretation, i.e., the presence of NiO on the surface of carbon only enhanced the adsorption of SO_2. So the pathway (A) might be the main route over the surface of sample Ni-AC.

3.5. NO removal tests

The selective catalytic reduction (SCR) of NO was tested using feed gas mixture $feed_{NO}$ (containing NO, NH_3 and O_2) in the reactor. The results are summarized in Fig. 7, where the NO conversion is plotted as one bar for each sample at each temperature level. At higher temperatures sample Cu-AC showed considerably higher activity compared to the other samples. However, at the lowest temperature, the V-AC showed the highest activity. The activity of Ce-AC remained high in the whole temperature range investigated by this study. It was interesting to find that the activity of samples AC, Fe-AC and Ni-AC varied according to the same trend. Meanwhile, samples containing Co and Mn showed negative NO reduction.

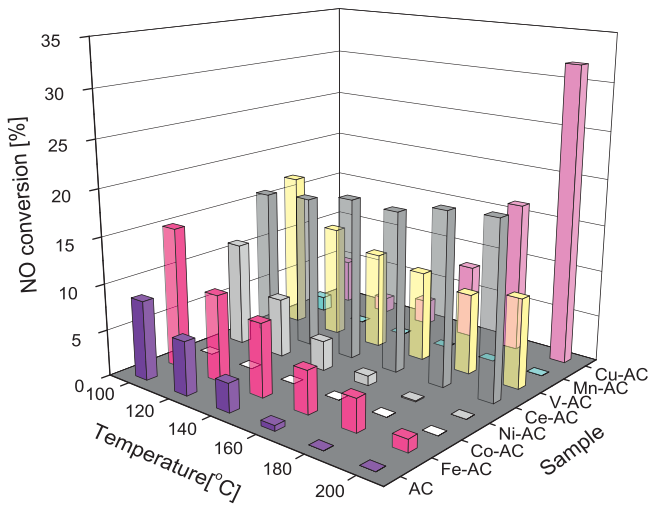

Fig. 7. NO conversion for the samples with $feed_{NO}$ gas mixtures. Negative values are not presented.

To ascertain the effect of doped metals in the activity, the kinetic rate constants per metal weight (k_m) were calculated. For oxygen partial pressures over 1 atm%, the SCR reaction can be considered to be approximately first order with respect to NO and zero order with respect to NH_3. Under these conditions the apparent rate constant (k_m) and the NO conversion (X) are related as follows [47],(1)$k_m = -\frac{F_0}{[NO]_0 W} \ln(1 - X)$, where F_0 is the molar NO feed rate (mol/s), $[NO]_0$ is the molar NO concentration at the inlet (mol/cm^3), and W is the weight of metal loaded. To eliminate the effect of carbon, the NO conversion was corrected for the support (by the subtraction of the conversion of AC from the corresponding values for the impregnated samples), and negative values are not involved.

Fig. 8 shows the Arrhenius plot, i.e., $\ln k_m$ vs. $1/T$. From the curves of samples Ce-AC, V-AC and Cu-AC, the apparent activation energies (E_a) and pre-exponential factors (k_0) were calculated. These are reported in Table 9. The lower activation energy of sample V-AC coincided with the higher activity at lower temperatures, while sample Cu-AC with higher activation energy showed the activity at higher temperatures, as can be seen in Fig. 7. As for samples Fe-AC and Ni-AC, the increase of temperature led to a decrease of the kinetic rate constant, and negative activation energies were obtained. This indicates that the process of NO adsorption rather

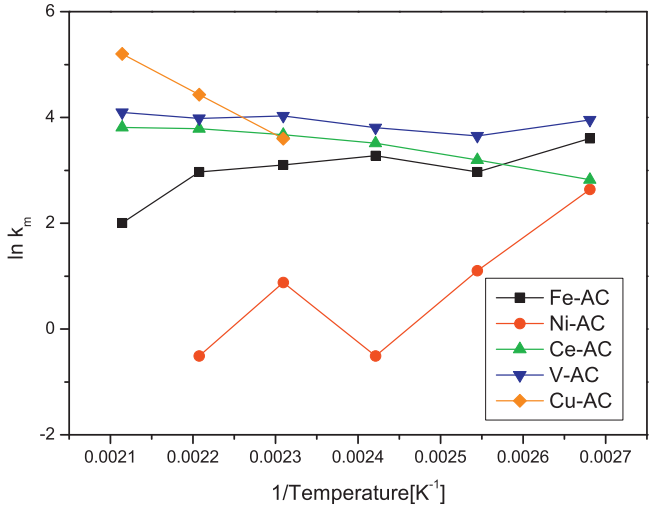

Fig. 8. Arrhenius plot ($\ln k_m$ vs. $1/T$) for the samples.

Table 9
Parameters of Arrhenius equation.

	Sample		
	Ce-AC	V-AC	Cu-AC
E_a (kJ mol^{-1})	14.73	3.84	68.20
k_0 (ccs^{-1} g^{-1})	2.175×10^3	1.512×10^2	6.166×10^9

than the catalytic one takes place on the surface of metal oxides in the temperature range of the experiments. This proposal was confirmed by Davini. He prepared the activated carbons impregnated with certain iron derivatives, and found these carbons showed good NO sorbent characteristic [6]. This finding could be used to account for the reason why the increase of temperature led to the decrease of NO conversion with respect to samples Fe-AC and Ni-AC, as well as AC, as shown in Fig. 7.

Based on these findings, the effect of metal on the NO removal could also be divided into three ways. First, metal catalyzed reduction of NO. The reduction potential of NO to N_2 is 1.678 V and N_2 to NH_3 is 0.057 V. Whether the catalytic reduction of NO is a feasible reaction over metal depends on the potential values of metal redox pairs. Their values should range from 0.057 to 1.678 V. Accordingly, Fe, Ce, V and Cu are candidates, as shown in Table 8. However, Fe-AC showed negative activation energy, and a higher reaction temperature might be needed. So the effect of Ce, V and Cu could be ascribed to catalytic reduction. Second, metal enhanced the adsorption of NO onto the carbon matrix. The effect of Ni-AC and Fe-AC could be ascribed to this type. As found in literature [11], NO chemisorption on the Ni-based catalyst led to the formation of highly stable NO complexes. With the increase of temperature, the effect would be lessened. Last, metal showed negative effect, like Mn and Co, due to the formation of NO from the NH_3 oxidation reaction, which competed with the SCR reaction. The same phenomena were also observed by Wallin et al. [48] and Marban et al. [12], respectively. In more detail, Marban concluded that MnO was a non-reactive oxide for the SCR reaction. Since Mn was present on the carbon surface in the form of MnO, as shown in the XPS results, the negative effect was not surprising.

In order to further investigate the specific activities of carbons impregnated with different metal oxides, the turnover frequencies were calculated assuming a first-order reaction rate [Eq. (2)] [47]. The turnover is defined as the number of moles of NO converted per mole of metal atom per minute.

$$\mathrm{TOF} = -\frac{F_0}{M}\ln(1-X), \tag{2}$$

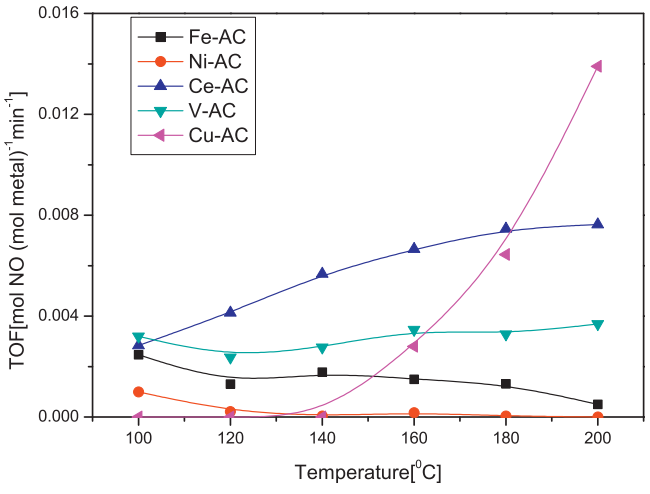

Fig. 9. TOF values of the samples versus the reaction temperatures.

where F_0 is the molar NO feed rate (mol/min), M is the moles of metals, and X is the conversion. The TOF values in the temperature range of the experiments are displayed in Fig. 9. It can be observed that the results coincide with the data of Figs. 7 and 8. Compared with V-AC, a better NO removal activity of Ce-AC in the temperature range of 100–200 °C was found. Since the vanadia catalyst is toxic, the Ce-containing catalyst seems to be a promising alternative.

4. Conclusion

Several metal oxides supported on an activated carbon using incipient wetness impregnation method were prepared. The impregnation of metal precursors followed by calcinations increased the specific surface as well as micropore volume for most of samples except Fe-AC and Ce-AC. XRD results showed that most metal oxides were well dispersed on the carbon matrix except V and Ce, due to particle aggregation upon heat treatment. XPS experiments were conducted to investigate the chemical state of metal on the carbon surface. Results showed that some metals (Cu and Fe) were partly reduced by carbon during preparation.

Based on different physicochemical properties, metal involved pathways for the SO_2 removal had been put out, i.e., catalytic oxidation, direct reaction and adsorption. This classification depended on the standard reduction potential values of metal redox pairs, which were identified by XPS results. The SO_2 removal tests revealed that the catalytic oxidation effect of the metal was crucial for SO_2 elimination. Of the metal oxides tested, V, Fe and Cu containing samples showed the better SO_2 removal performance due to their catalytic properties.

The SCR activity of the samples was tested using feed gas mixture $feed_{NO}$ (containing NO, NH_3 and O_2) in the same reactor. Samples impregnated with V, Ce and Cu showed good activity for NO reduction by NH_3, whereas the deposition of Fe and Ni enhanced the adsorption of NO rather than reduction ability. Samples containing Co and Mn showed negative effect of NO removal. The different performances were also ascribed to the standard reduction potential values of metal redox pairs. A metal cation which could easily convert between the two valences seemed to be crucial to the good performance of SO_2 and NO removal, just like V and Cu. Of the metals investigated, Ce seemed to be a promising alternative to V due to the higher activity and the nontoxic property.

Acknowledgements

We gratefully acknowledge the financial support of the National Natural Science Foundation of China (No. 50776079) and Development of China (863 Program) (No. 2007AA061802).

References

[1] M.A. Daley, C.L. Mangun, J.A. DeBarr, S. Riha, A.A. Lizzio, G.L. Donnals, J. Economy, Adsorption of SO_2 onto oxidized and heat-treated activated carbon fibers (ACFS), Carbon 35 (1997) 411–417.
[2] S.V. Vassilev, C. Braekman-Danheux, R. Moliner, I. Suelves, M.J. Lazaro, T. Thiemann, Low cost catalytic sorbents for NOx reduction. 1. Preparation and characterization of coal char impregnated with model vanadium components and petroleum coke ash, Fuel 81 (2002) 1281–1296.
[3] Y. Xiao, Q.Y. Liu, Z.Y. Liu, Z.G. Huang, Y.X. Guo, J.L. Yang, Roles of lattice oxygen in V_2O_5 and activated coke in SO_2 removal over coke-supported V_2O_5 catalysts, Appl. Catal. B: Environ. 82 (2008) 114–119.
[4] P. Davini, The effect of certain metallic derivatives on the adsorption of sulphur dioxide on active carbon, Carbon 39 (2001) 419–424.
[5] J. Klinik, T. Grzybek, The influence of the addition of cobalt, nickel, manganese and vanadium to active carbons on their efficiency in SO_2 removal from stack gases, Fuel 71 (1992) 1303–1308.
[6] P. Davini, SO_2 and NOx adsorption properties of activated carbons obtained from a pitch containing iron derivatives, Carbon 39 (2001) 2173–2179.
[7] J.R. Ma, Z.Y. Liu, S.J. Liu, Z.P. Zhu, A regenerable Fe/AC desulfurizer for SO_2 adsorption at low temperatures, Appl. Catal. B: Environ. 45 (2003) 301–309.

[8] H.H. Tseng, M.Y. Wey, Study of SO_2 adsorption and thermal regeneration over activated carbon-supported copper oxide catalysts, Carbon 42 (2004) 2269–2278.
[9] Z.P. Zhu, Z.Y. Liu, H.X. Niu, S.J. Liu, Promoting effect of SO_2 on activated carbon-supported vanadia catalyst for NO reduction by NH_3 at low temperatures, J. Catal. 187 (1999) 245–248.
[10] Z.P. Zhu, Z.Y. Liu, S.J. Liu, H.X. Niu, A novel carbon-supported vanadium oxide catalyst for NO reduction with NH_3 at low temperatures, Appl. Catal. B: Environ. 23 (1999) L229–L233.
[11] G. Marban, R. Antuna, A.B. Fuertes, Low-temperature SCR of NOx with NH_3 over activated carbon fiber composite-supported metal oxides, Appl. Catal. B: Environ. 41 (2003) 323–338.
[12] G. Marban, T. Valdes-Solis, A.B. Fuertes, Mechanism of low temperature selective catalytic reduction of NO with NH_3 over carbon-supported Mn_3O_4 – active phase and role of surface NO species, Phys. Chem. Chem. Phys. 6 (2004) 453–464.
[13] G. Marban, T. Valdes-Solis, A.B. Fuertes, Mechanism of low-temperature selective catalytic reduction of NO with NH_3 over carbon-supported Mn_3O_4 – role of surface NH_3 species: SCR mechanism, J. Catal. 226 (2004) 138–155.
[14] J. Pasel, P. Kassner, B. Montanari, M. Gazzano, A. Vaccari, W. Makowski, T. Lojewski, R. Dziembaj, H. Papp, Transition metal oxides supported on active carbons as low temperature catalysts for the selective catalytic reduction (SCR) of NO with NH_3, Appl. Catal. B: Environ. 18 (1998) 199–213.
[15] G.S. Szymanski, T. Grzybek, H. Papp, Influence of nitrogen surface functionalities on the catalytic activity of activated carbon in low temperature SCR of NOx with NH_3, Catal. Today 90 (2004) 51–59.
[16] Z.P. Zhu, Z.Y. Liu, S.J. Liu, H.X. Niu, T.D. Hu, T. Liu, Y.N. Xie, NO reduction with NH_3 over an activated carbon-supported copper oxide catalysts at low temperatures, Appl. Catal. B: Environ. 26 (2000) 25–35.
[17] D. Lopez, R. Buitrago, A. Sepulveda-Escribano, F. Rodriguez-Reinoso, F. Mondragon, Low temperature catalytic adsorption of SO_2 on activated carbon, J. Phys. Chem. C 112 (2008) 15335–15340.
[18] X. Li, V.E. Henrich, Reaction of SO_2 with stoichiometric and defective NiO(1 0 0) surfaces, Phys. Rev. B 48 (1993) 17486–17492.
[19] K. Kante, E. Deliyanni, T.J. Bandosz, Interactions of NO_2 with activated carbons modified with cerium, lanthanum and sodium chlorides, J. Hazard. Mater. 165 (2009) 704–713.
[20] J. Muniz, J.E. Herrero, A.B. Fuertes, Treatments to enhance the SO_2 capture by activated carbon fibres, Appl. Catal. B: Environ. 18 (1998) 171–179.
[21] E. Garcia-Bordeje, M.J. Lazaro, R. Moliner, P.M. Alvarez, V. Gomez-Serrano, J.L.G. Fierro, Vanadium supported on carbon coated honeycomb monoliths for the selective catalytic reduction of NO at low temperatures: influence of the oxidation pre-treatment, Carbon 44 (2006) 407–417.
[22] D. Nguyen-Thanh, T.J. Bandosz, Effect of transition-metal cations on the adsorption of H_2S in modified pillared clays, J. Phys. Chem. B 107 (2003) 5812–5817.
[23] Y.W. Lee, J.W. Park, J.H. Choung, D.K. Choi, Adsorption characteristics of SO_2 on activated carbon prepared from coconut shell with potassium hydroxide activation, Environ. Sci. Technol. 36 (2002) 1086–1092.
[24] B. Rubio, M.T. Izquierdo, Influence of low-rank coal char properties on their SO_2 removal capacity from flue gases. 1. Non-activated chars, Carbon 35 (1997) 1005–1011.
[25] Z. Liu, A.Q. Wang, X.D. Wang, T. Zhang, Ir–C xerogels synthesized by sol–gel method for NO reduction, Catal. Today 137 (2008) 162–166.
[26] F.J. Maldonado-Hodar, C. Moreno-Castilla, J. Rivera-Utrilla, Y. Hanzawa, Y. Yamada, Catalytic graphitization of carbon aerogels by transition metals, Langmuir 16 (2000) 4367–4373.
[27] Y.C. Xie, Y.Q. Tang, Spontaneous monolayer dispersion of oxides and salts onto surfaces of supports: applications to heterogeneous catalysis, Adv. Catal. 37 (1990) 1–47.
[28] X.Y. Guo, C. Bartholomew, W. Hecker, L.L. Baxter, Effects of sulfate species on V_2O_5/TiO_2 SCR catalysts in coal and biomass-fired systems, Appl. Catal. B: Environ. 92 (2009) 30–40.
[29] M. Pakula, S. Biniak, A. Swiatkowski, Chemical and electrochemical studies of interactions between iron(III) ions and an activated carbon surface, Langmuir 14 (1998) 3082–3089.
[30] C. Moreno-Castilla, F.J. Maldonado-Hodar, A.F. Perez-Cadenas, Physicochemical surface properties of Fe, Co, Ni, and Cu-doped monolithic organic aerogels, Langmuir 19 (2003) 5650–5655.
[31] Z. Konya, J. Kiss, A. Oszko, A. Siska, I. Kiricsi, XPS characterisation of catalysts during production of multiwalled carbon nanotubes, Phys. Chem. Chem. Phys. 3 (2001) 155–158.
[32] C.D. Wagner, W.M. Riggs, L.E. Davis, J.F. Moulder, G.E. Muilenberg, Handbook of X-ray Photoelectron Spectroscopy, Perkin-Elmer Physical Electronics Division, Eden Prairier, MI, 1978.
[33] http://srdata.nist.gov/xps.
[34] E. Garcia-Bordeje, J.L. Pinilla, M.J. Lazaro, R. Moliner, J.L.G. Fierro, Role of sulphates on the mechanism of NH_3-SCR of NO at low temperatures over presulphated vanadium supported on carbon-coated monoliths, J. Catal. 233 (2005) 166–175.
[35] A. Laachir, V. Perrichon, A. Badri, J. Lamotte, E. Catherine, J.C. Lavalley, J. Elfallah, L. Hilaire, F. Lenormand, E. Quemere, G.N. Sauvion, O. Touret, Reduction of CeO_2 by hydrogen-magnetic-susceptibility and Fourier-transform infrared, ultraviolet and X-ray photoelectron-spectroscopy measurements, J. Chem. Soc. 87 (1991) 1601–1609.
[36] F. Larachi, J. Pierre, A. Adnot, A. Bernis, Ce 3d XPS study of composite $Ce_xMn_{1-x}O_{2-y}$ wet oxidation catalysts, Appl. Surf. Sci. 195 (2002) 236–250.
[37] L.F. Liotta, G. Di Carlo, G. Pantaleo, A.M. Venezia, G. Deganello, Co_3O_4/CeO_2 composite oxides for methane emissions abatement: relationship between Co_3O_4–CeO_2 interaction and catalytic activity, Appl. Catal. B: Environ. 66 (2006) 217–227.
[38] P.C.C. Faria, J.J.M. Orfao, M.F.R. Pereira, A novel ceria-activated carbon composite for the catalytic ozonation of carboxylic acids, Catal. Commun. 9 (2008) 2121–2126.
[39] E. Raymundo-Piñero, D. Cazorla-Amorós, C. Salinas-Martinez de Lecea, A. Linares-Solano, Factors controlling the SO_2 removal by porous carbons: relevance of the SO_2 oxidation step, Carbon 38 (2000) 335–344.
[40] P. Davini, Adsorption and desorption of SO_2 on active-carbon—the effective of surface basic groups, Carbon 28 (1990) 565–571.
[41] F. Carrascomarin, E. Utrerahidalgo, J. Riverautrilla, C. Morenocastilla, Adsorption of SO_2 in flowing air onto activated carbons from olive stones, Fuel 71 (1992) 575–578.
[42] A.A. Lizzio, J.A. DeBarr, C.W. Kruse, Production of activated char from Illinois coal for flue gas cleanup, Energy Fuels 11 (1997) 250–259.
[43] N.R. Urban, K. Ernst, S. Bernasconi, Addition of sulfur to organic matter during early diagenesis of lake sediments, Geochim. Cosmochim. Acta 63 (1999) 837–853.
[44] J. Zawadzki, Infrared studies of SO_2 on carbons—II. The SO_2 species adsorbed on carbon-films, Carbon 25 (1987) 495–502.
[45] Z.P. Zhu, NO Reduction over Activated Coke Supported Metal Oxides Catalysts at Low Temperatures, Chinese Academy of Sciences, Taiyuan, 2002.
[46] G. Milazzo, S. Caroli, R.D. Braun, Tables of standard electrode potentials, J. Electrochem. Soc. 125 (1978) 261C.
[47] E. Garcia-Bordeje, M.J. Lazaro, R. Moliner, J.F. Galindo, J. Sotres, A.M. Baro, Structure of vanadium oxide supported on mesoporous carbon-coated monoliths and relationship with its catalytic performance in the SCR of NO at low temperatures, J. Catal. 223 (2004) 395–403.
[48] M. Wallin, S. Forser, P. Thormahlen, M. Skoglundh, Screening of TiO_2-supported catalysts for selective NOx reduction with ammonia, Ind. Eng. Chem. Res. 43 (2004) 7723–7731.